applied sciences

MDPI

Special Issue Paper

Time-Sequential Working Wavelength-Selective Filter for Flat Autostereoscopic Displays

René de la Barré [1,*], Roland Bartmann [1], Silvio Jurk [1], Mathias Kuhlmey [1], Bernd Duckstein [1], Arno Seeboth [2], Detlef Lötzsch [2], Christian Rabe [2], Peter Frach [3], Hagen Bartzsch [3], Matthias Gittner [3], Stefan Bruns [4], Gerhard Schottner [5] and Johanna Fischer [5]

[1] Department of Vision & Imaging Technologies, Fraunhofer Institute for Telecommunications, Heinrich Hertz Institute HHI, 10587 Berlin, Germany; roland.bartmann@hhi.fraunhofer.de (R.B.); silvio.jurk@hhi.fraunhofer.de (S.J.); mathias.kuhlmey@hhi.fraunhofer.de (M.K.); bernd.duckstein@hhi.fraunhofer.de (B.D.)

[2] Department of Chromogenic Polymers, Fraunhofer Institute for Applied Polymer Research IAP, 12489 Berlin, Germany; arno.seeboth@iap.fraunhofer.de (A.S.); detlef.loetzsch@iap.fraunhofer.de (D.L.); christian.rabe@iap.fraunhofer.de (C.R.)

[3] Department of Precision Coatings, Fraunhofer Institute for Organic Electronics, Electron Beam and Plasma Technology FEP, 01109 Dresden, Germany; peter.frach@fep.fraunhofer.de (P.F.); hagen.bartzsch@fep.fraunhofer.de (H.B.); matthias.gittner@fep.fraunhofer.de (M.G.)

[4] Department of Optical and Electrical Coatings, Fraunhofer Institute for Surface Engineering and Thin Films IST, 38108 Braunschweig, Germany; stefan.bruns@ist.fraunhofer.de

[5] Business Unit Surfaces and Coatings, Fraunhofer Institute for Silicate Research ISC, 97082 Würzburg, Germany; gerhard.schottner@isc.fraunhofer.de (G.S.); johanna.fischer@isc.fraunhofer.de (J.F.)

* Correspondence: rene.de_la_barre@hhi.fraunhofer.de; Tel.: +49-30-3100-2345

Academic Editors: Nasser Peyghambarin and Yeshaiahu Fainman
Received: 15 December 2016; Accepted: 10 February 2017; Published: 16 February 2017

Abstract: A time-sequential working, spatially-multiplexed autostereoscopic 3D display design consisting of a fast switchable RGB-color filter array and a fast color display is presented. The newly-introduced 3D display design is usable as a multi-user display, as well as a single-user system. The wavelength-selective filter barrier emits the light from a larger aperture than common autostereoscopic barrier displays with similar barrier pitch and ascent. Measurements on a demonstrator with commercial display components, simulations and computational evaluations have been carried out to describe the proposed wavelength-selective display design in static states and to show the weak spots of display filters in commercial displays. An optical modelling of wavelength-selective barriers has been used for instance to calculate the light ray distribution properties of that arrangement. In the time-sequential implementation, it is important to avoid that quick eye or eyelid movement leads to visible color artifacts. Therefore, color filter cells, switching faster than conventional LC display cells, must distribute directed light from different primaries at the same time, to create a 3D presentation. For that, electric tunable liquid crystal Fabry–Pérot color filters are presented. They switch on-off the colors red, green and blue in the millisecond regime. Their active areas consist of a sub-micrometer-thick nematic layer sandwiched between dielectric mirrors and indium tin oxide (ITO)-electrodes. These cells shall switch narrowband light of red, green or blue. A barrier filter array for a high resolution, glasses-free 3D display has to be equipped with several thousand switchable filter elements having different color apertures.

Keywords: fast switchable wavelength-selective elements; autostereoscopic image splitter; color filter barrier array; computational display; Fabry–Pérot color filter; on-off filter mode

1. Introduction

Optical image splitters are often used to build autostereoscopic displays. A high number of image splitter elements is necessary to shorten the internal projection way and to create tiny projections on the level of pixels and subpixels. That causes a flat 3D display design. Some switchable techniques allow an opening and closing of alternative barrier apertures on the image splitter. These components are known as spatial light modulators [1].

The image splitter is placed either directly in front or behind the pixel plane of the display panel. Common forms of image splitters are parallax barrier and lenticular lens arrays [2]. Special kinds of barriers are wavelength-selective [3–5]. Stripe, step and hole masks complete the possible geometric shapes of the barrier and can be designed with various ratios and slant angles.

Autostereoscopic multiview displays are distinguished in several techniques characterized by the geometrical relation of the display and image splitter [1,2,6]. Therefore, classifications differ in two-view, multiview and light field displays.

Response times of tunable color filters and optical color shutters in the millisecond regime enable novel applications already in the area of image recording, image displaying and processing of video sources [7–9]. The strong birefringence of liquid crystals, the possibility to align them by confining surfaces and to trigger their alignment by an external electric field makes them well suitable for tunable interference filters [10–12]. The reorientation of nematic liquid crystals (NLCs) has been proven in various interference filter designs to generate fast switching times and wide shifting ranges. These include Lyot filter stacks [13,14] and the Fabry–Pérot filter [11,15,16]. A Lyot filter stack consists of several stages of a birefringent layer and a subsequent polarizer, whereby the birefringent layer of each stage has half the thickness of the preceding one. Electrically-tunable NLC Lyot filter stacks operating in the visible light range were already commercialized [12].

In this paper, we report a novel barrier technique for autostereoscopic displays using fast switchable wavelength-selective filters as time-sequential image splitter elements. In the following sections, we describe the methodology of designing wavelength-selective filter barriers for autostereoscopic displays. We outline two example solutions we have found with the applied search strategy. We show an experimental setup for the assessment of the design, and we report about an experimental evaluation of a fast switching cell design with Fabry–Pérot characteristics.

2. Switchable Color Filter Barrier for Autostereoscopic Display Design

The autostereoscopic 3D displays discussed in this paper use a time-sequential switchable wavelength-selective filter barrier. Stripe-patterned filters with different transmittance ranges are used for the directional separation of multiple stereoscopic image information. The visibility of visual artifacts will be avoided by the transmission of all display colors in every light-emitting step of the sequence.

2.1. Basic Structure of Switchable Wavelength-Selective Barriers for Multiview 3D Display

Figure 1 illustrates schematically the cross-section of such an autostereoscopic 3D display. The Blue-Green-Red (BGR) color filter barrier *FP* is positioned at a selected grid distance *a* in front of an RGB pixel matrix plane *PMP*. Such multiview displays emit directionally different image information into neighbored viewing zones of width *P*. For this purpose, the screen was divided into image strips where the individual views are interleaved on the subpixel level. Each image strip *VP* with a width of *n* subpixels, *SP* contains information of every view in its neighboring pixel columns.

Switchable color filters can be applied as a shift filter and an on/off filter. In the example shown in Figure 1, the color filter elements are not able to change their passband. In the on-state, their individual barrier elements transmit only one of the red, green or blue wavelength ranges, and in the off-state, they block all visible light. Optimal dimensions and the appropriate arrangement of the barrier cause the emitted light rays to converge at the viewing distance *D* on the image projection plane *PP*.

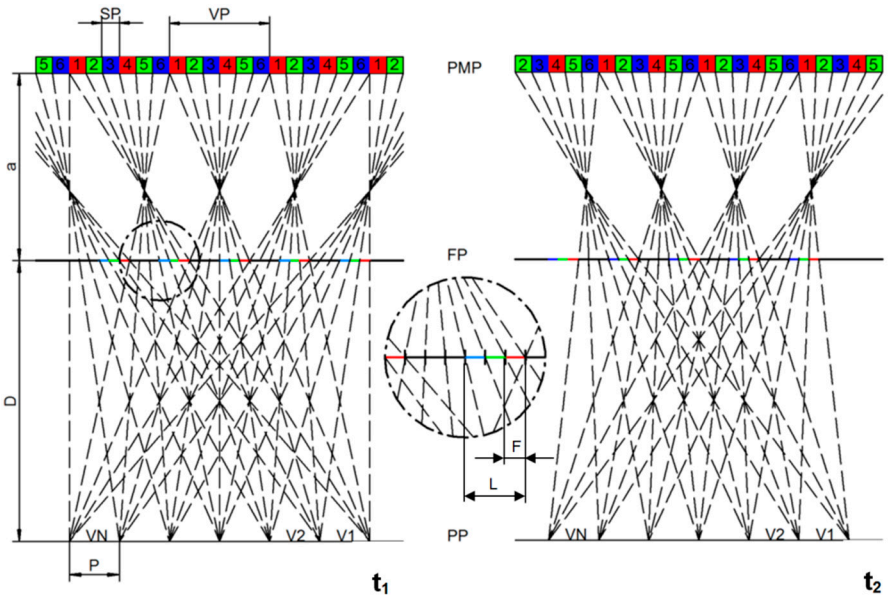

Figure 1. Principle of time-sequential operation of a wavelength-selective multiview 3D display at the state at t_1 and t_2 with resolution enhancement in the same positioned viewing zones *V*1 to *VN*.

For this purpose, the individual filter elements of the width *F* need a certain period width *L*. They are arranged in a period that is slightly smaller than the width of the image-strip *VP*. The views correspond to the *n* subpixels, which will be visible in one of the channels *V*1 to *VN*. Because of the time-sequential mode, the details of a number of different interlaced images corresponding to the number of switching states will be visible. This increases the resolution of views and is proportional to the number of switching stages of the alternative filter elements.

Common layouts of autostereoscopic barrier displays use a slanted barrier and a standard 2D matrix display. In contrast, we decided to use a vertical color stripe barrier and a display matrix with vertically-alternating subpixel colors. Figure 2 shows this arrangement. The color stripe pattern of the barrier is exactly rectangular oriented to the colors on the display matrix. Subpixels with the same color are located in a row. Therefore, a local emission in one of the colors does not show any change of brightness at the movement of the observer within a lobe. A time-sequentially switchable, wavelength-selective RGB-color-filter barrier *FP* was placed at a defined distance *a* in front of the matrix display. In this arrangement, the contents of the left and right views were interleaved line-by-line separated always by one color. Figure 2 shows how the left view, drawn with the brighter colors, and the right view, drawn with the darker colors, were interlaced with always three neighboring subpixels of the same color per line. From line to line, the position in the content changes by two subpixels, because of the same offset of the colors in the barrier. As in Figure 1, on this 3D display design, the same parameter $V = 6$ can be defined as the number of subpixel per group *VP*, but this separated for every color.

The emitted light converges at viewing distance *D* in adjacently arranged stereo rhombs of uniform color mixing of red, green and blue. Figure 2 demonstrates the time-sequential operating mode, where alternative openings are created and the subpixel allocation is simultaneously shifted by *V*/2 subpixels. Opposite the arrangement in Figure 1, the color filter stripes are equally distributed anytime. The shift does ensure that the image contents of the adjacent stereo zones converge at the same position [17,18].

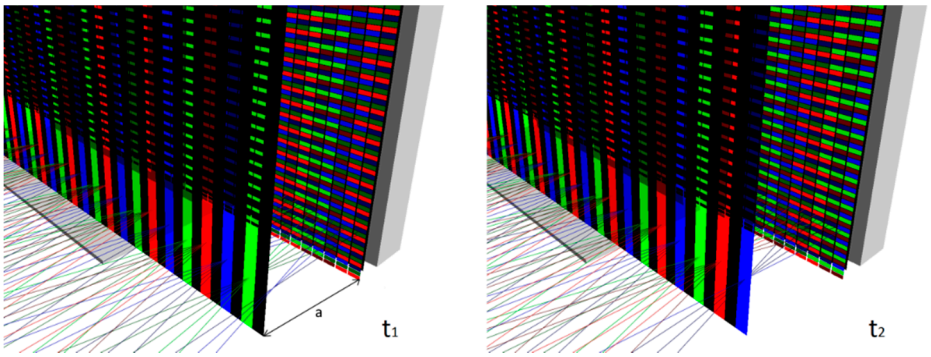

Figure 2. Partial view on the setup of the time-sequential wavelength-selective 3D display. The depicted colored light-rays are transmitted through the corresponding color filter stripes. The presentations on the left and right show the two switching states at times t_1 and t_2.

2.2. Geometric Considerations

Figure 3 schematically illustrates a cross-sectional view of the 3D display shown in Figure 2 for a row of red subpixels and its associated red filter barriers.

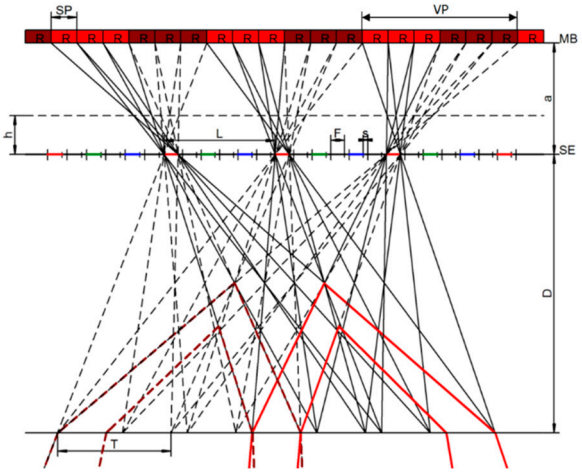

Figure 3. Top view, horizontal cross-section of the display design for single-user mode. The left and the right view share always six red subpixels per group *VP* [19] (© Fraunhofer HHI).

The border rays from the subpixels of width *SP* pass the red barrier at distance a. It is shown exemplarily how the projections of the rays from dark red drawn subpixels mark a channel *T*. For that purpose, the ratio *R* between subpixel width *SP* and the filter width *F*, as well as the width of the gap *s*, has to be well designed. *R* indicates whether the presentation of a 3D display converges like for a multiview or two-view display. In these cases, the ratio has to be by $R > 1$ [3]. It can be calculated by distance *L* between the opened color filters of identical wavelength and of image strip width *VP* or from viewing distance *D* and grid distance *a*.

$$R = \frac{SP}{F+s} = \frac{VP}{L} = \frac{D+a}{D} \tag{1}$$

The channel width *T*, which derives from the viewing distance *D*, can be calculated with the following Equation (2). This equation describes the width of every stereo zone. Figure 3 shows a single-user 3D display with three bundled subpixels in one stereo channel. Two stereo rhombs are created and overlapped by 1/3 of their projection width *T*. The central area of such a stereo-zone has no optical crosstalk.

$$T = \frac{(a+D)\cdot(F+SP)}{a} - SP \tag{2}$$

To minimize crosstalk and thus to achieve a better separation gap, s can be embedded between the filter barriers. These gaps reduce the crosstalk, but also the luminance efficiency [19].

2.3. Switching Mode

In time-sequential operating mode, the writing of interlaced content into the display panel and the shift of the filter barrier have to be synchronized. The display pixels in the LC cells are not illuminated by the backlight before their switching operations are completed. Otherwise, the image content of the previous stereo image would be still visible and lead to crosstalk. Although, a more simple structure of the switchable filter is possible if the display panel is rotated by 90 degrees: the screen layout no longer runs from top to bottom, but from left to right.

The barrier strips are also switched from the left to the right. Since the switching process of the filter barrier is matching the writing direction of the display, the display panel, filter barrier and backlight can be synchronized in a rolling shutter operation mode. That requires very fast switching filter barriers and displays. The cross-talk will be minimized during switching by the progressive motion of the blanking phase BP from the left to the right, in which the backlight is switched and localized to black. The required switching speed of the components results from the need to finish the optical switching processes of corresponding image and filter columns within this dark phase. So the system timing is determined by the slowest response time of the on/off-times. A simple control scheme is possible when the length of the screen time BZ and blanking phase BP are equal. The frame rate is then determined by the half number of interlaced images written in the display. The number of different switching stages of the wavelength-selective filter specifies an image sequence. This sequence is reproduced with a frequency on the display, which ensures a flicker-free image representation. In the simplest case with two switching stages and two blanking periods, always repeated 60 times, the frequency for writing the images would be 240 Hz. [20].

The local white balance, realized by summation of neighboring colors can be guaranteed in each switching stage, if their number is not a multiple of the number N_c of primary colors. At the same time, all opened slots transmit the same color, if the number of switching stages v_s is a multiple of N_c. The white balance can be achieved only time-sequentially, which is visible at fast eye movements (saccades) as color breakup. A circumvention of this limitation is described in the chapter about the multiview mode.

2.4. Resolution and Luminance

The maximum resolution achievable by the time-sequential operating mode is the full resolution in the horizontal direction and $1/N_c$ in the vertical direction. The maximum luminance L_{max}, which can be achieved at optimal transmission of the filter elements, is dependent on the number of switching operations v_s and the length of the blanking period BP. The general relationship is shown in the following Equation (3).

$$L_{\max} = \frac{L_{\mathrm{RGB}}}{N_c \cdot \nu_s \cdot \left(\frac{BP}{BZ} + 1\right)} \tag{3}$$

The parameter L_{RGB} is the luminance of the full emitting display panel. In comparison with black and white barriers, the resulting luminance L_{max} is the same, but the resolution is improved. However, using a blanking period BP identical to the screen time BZ, the luminance is reduced.

2.5. Two View Mode

The display design shown in Figure 3 is carried out in Figure 4 for the two-view mode. The interleaving pattern and the overlaid filter barrier are illustrated for a display with six subpixels per subpixel group and two switching stages. The arrangements correspond to the time-sequential steps of operation in an autostereoscopic single-user display.

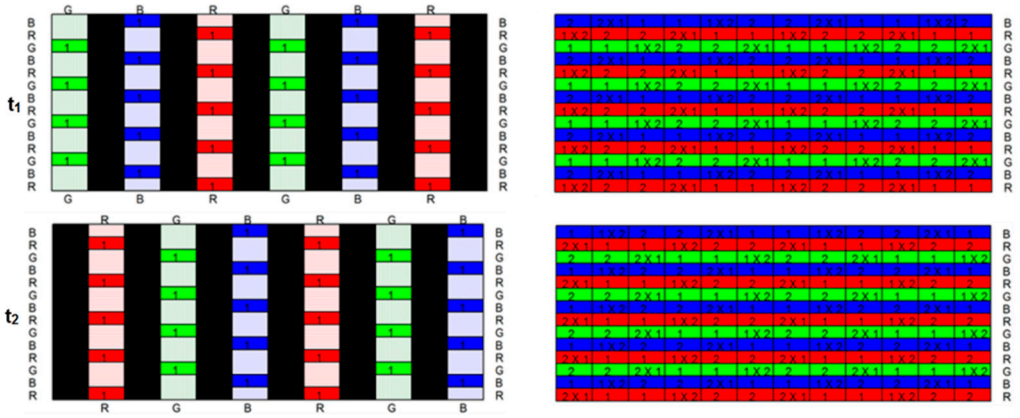

Figure 4. Left side: wavelength-selective filter barrier in two switching stages t_1 and t_2; **right side**: the corresponding interleaving of the image contents of the left view (1) and the right view (2) and its mixes (1*X*2 and 2*X*1).

The contents of left view (1) and right view (2) are dedicated to the available subpixels within subpixel-groups *VP*. As illustrated in Figure 4, through the color barriers, the left content is visible to one eye. The other eye sees the right content. Subpixels covered by the blanked filter stripes are used for mixing of the content. As sign for mixing is an *x* used. If the user moves his/her head, mixing ratios and positions of mixed subpixels change depending on the user position. This is effectuates by a tracking signal. The switching stages effect a horizontal offset of three subpixels between the interleaving patterns.

The configuration of the filter barriers can be freely selected without changing the basic structure of the display. Thus, additional switching stages will be generated with other filter assignments to control the width of the stereo zone or the value of the optical crosstalk. The interleaving pattern and the frame rate of the display or the readout frequency of the image memory have to be adapted to the respective configuration. This can be adapted precise in the *X*–*Z* direction to the eye position of the observer. An accurate redistribution of the image content is required. For this purpose, the bordering subpixels I_{1X2} and I_{2X1} located between the left I_1 and right I_2 image content are interpolated proportionally in dependence of the displacement value I_s according to the Equations (4) and (5). The offset value I_s is a floating point number. The fractional part of the offset value determines the interpolation ratio [20]. Furthermore, other approaches for a redistribution of brightness intensities of the views are possible [21].

$$I_{1X2} = I_1 \cdot (I_s - \lfloor I_s \rfloor) + I_2 \cdot (1 - (I_s - \lfloor I_s \rfloor)) \quad (4)$$

$$I_{2X1} = I_2 \cdot (I_s - \lfloor I_s \rfloor) + I_1 \cdot (1 - (I_s - \lfloor I_s \rfloor)) \quad (5)$$

The emission characteristic of this display design was tested in a ray-tracing simulation developed for wavelength-selective 3D displays. Narrowband filters and no refractive optics are used. The simulation software could be limited to the determination of the radiation behavior from the superposition in the three core wavelengths. Modeling of the subpixels, their matrix and the color filter barrier is based on geometrical optics and a Lambertian radiator approximation of higher order [7].

The luminance profiles and, thus, the emission properties of each stereo channel are position dependent. Their determination depends on the special design (geometry and color) of the filter barrier and the necessary content distribution [18]. The luminance profiles for a single-user display shown in Figure 5 are the result of such simulation. They correspond to an idealized description of color filters, which have an optimal transmission characteristic. Only light of the corresponding wavelengths will pass the filter barrier.

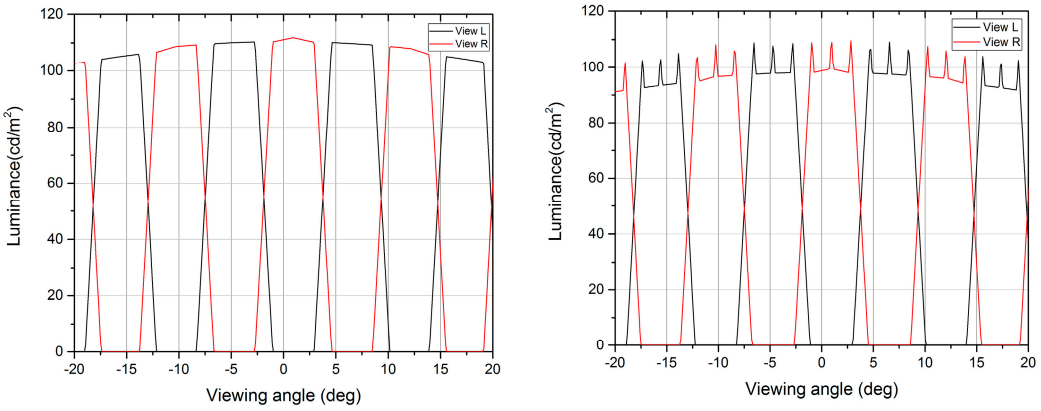

Figure 5. Luminance profiles for a two-view display design, **left** without gaps and **right** with gaps on the subpixel matrix.

At first, the display matrix is modeled with rectangular subpixels without a gap. In combination with the vertically-oriented filter barrier, a nearly rectangular gradient of intensity results on the imaging plane, only similar to lenticular lens grids. Therefore, separation of the left and right image content is improved. The increase in crosstalk at larger viewing angles remains moderate. In contrast to the lenticular lens raster, there is no angle-dependent field curvature, the Petzval curve, of the focal point. An angle-dependent decrease in brightness can be read from the diagram. It is determined by the emission characteristic of the pixel panel.

Second, the calculation uses vertical gaps with 10% of the width of the original pixel height. The resulting graph shows that a 10% gap reduces the brightness similarly by about the same percentage.

2.6. n-View Mode

In the case of switching the above display design to an *n*-view multiview 3D display, all subpixels of a subpixel group will be assigned with more than two slightly different partial images of a scene. Those will be interleaved, dependent on the number of switching steps with a line-by-line offset.

The images in Figure 6 show a multiview 3D display with nine views and three switching steps, where the left side shows the filter state of the entire system and the right side the associated interleaving pattern. The number of switching steps, three, corresponds to an RGB-color barrier. White compensation is possible by superposition of the colors in the time domain. A local summation of all three colors is realized by switching the filter colors in accordance to the step number in multiples of three. In this special case, the sequence of nine filters belonging to one subpixel group would be changed from RGB-RGB-RGB into RGB-GBR-BRG.

Figure 7 shows the luminance profiles for the nine view multiview 3D display as described above. This display design also was simulated and evaluated by the simulation tool. Due to a vertically-aligned grid and horizontally-arranged subpixel, the luminance profiles of each view get a triangle shape. In the center of each view, the luminance profiles reach their maxima, because there is only one single point in front of that display, where the whole area of a subpixel exactly shines through the aperture. On this system, we also realize that there is a linear changing of image information of views 1–9. The display approach works therefore like a continuous multiview system. The maximal intensity of a view is 111 cd/m², implied by Equation (3), where the initial luminance is L_{RGB} = 1000 cd/m² and the number of switching steps are v_s = 3.

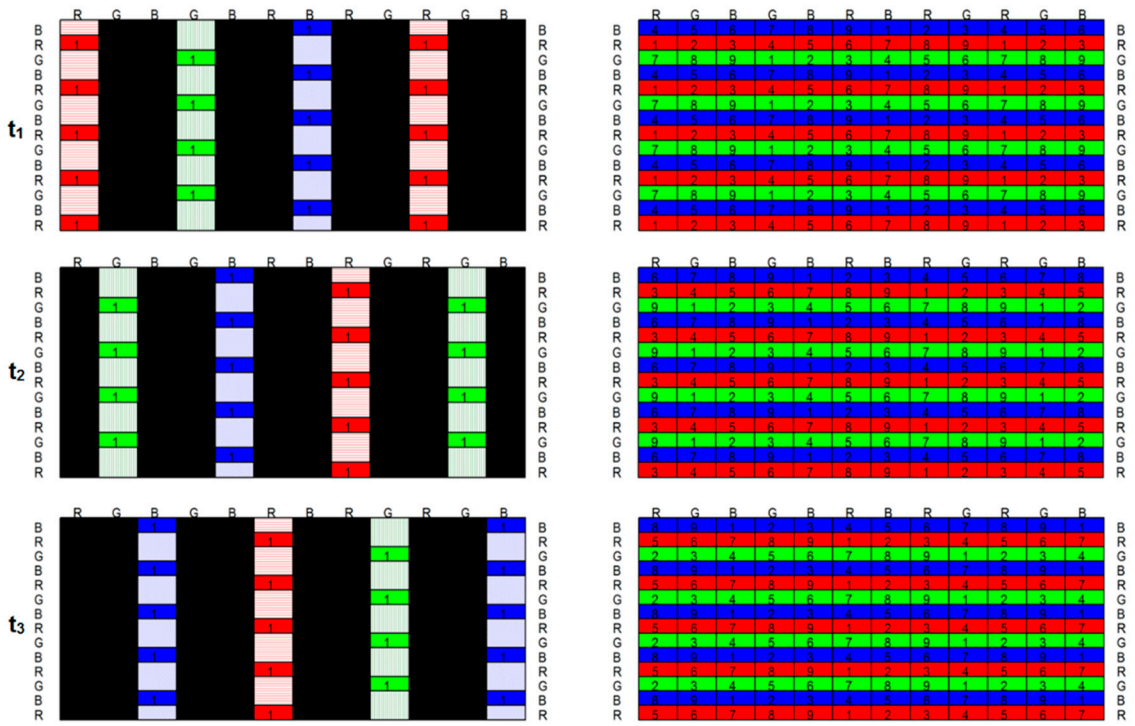

Figure 6. Multiview mode with special color filter scheme by using nine views and three switching stages (at the times t_1, t_2, t_3); on the **left side** is illustrated the color filters and on the **right side** the corresponding interleaving pattern.

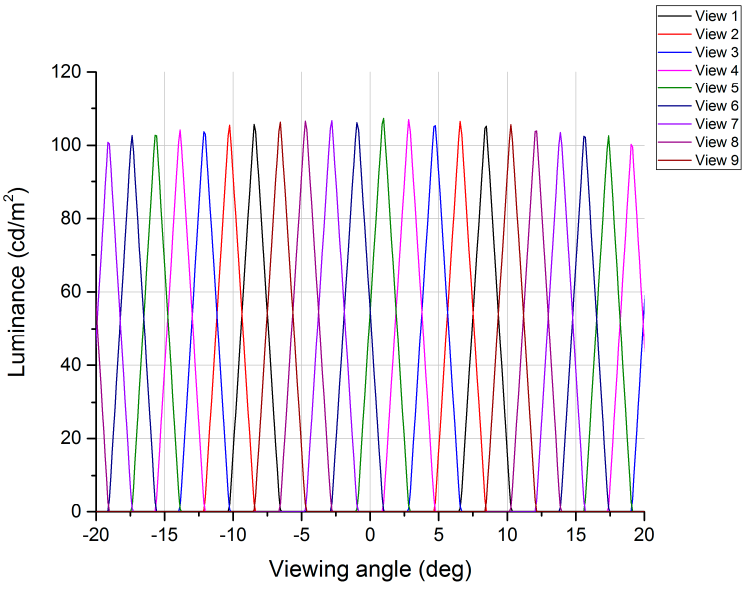

Figure 7. Luminance profiles for the nine views of the multiview display design.

3. Experiments and Results

3.1. Verification of Switchable Color Filter Array Assembled with a Large Area Color Display

The display design of an autostereoscopic screen with a switchable wavelength-selective parallax-barrier was set up by commercially available display components. It was experimentally examined how the theoretical approach corresponds to the practical behavior.

The double-display mock-up is based on two different flat screens and is shown in Figure 8. Resolution data and pixel pitches of the display are listed in Table 1. In reference to the chosen

display design, continuous RGB-color lines are arranged by 90°-twisting of the rear Display 1. The interspace distance between both displays can be aligned by micrometer screws at four positions. For the investigations, the distance *a* between display and barrier is set to 2.9 mm. This display combination shows a central-perspective emission characteristic as needed for multiview technologies. Both displays use nematic crystals and in-plane-switching technology with a 1:3 aspect ratio of pixel shape. The opposite arranged polarizers of the displays are aligned in the same direction. The 3D display arrangement in operation shows visible moiré-formation caused by the overlapping of two periodical grids and the high area share in subpixel gap lines. To suppress those effects, the usage of elliptical diffusors was examined. However, the reduction of moiré-effects by diffusion affects the image contrast.

Table 1. Display data.

Device	Resolution	Pixel-Pitch
Display 1	5120 × 2880 (5 K)	11,655 µm
Display 2	1366 × 720 (1.4 K)	34,950 µm

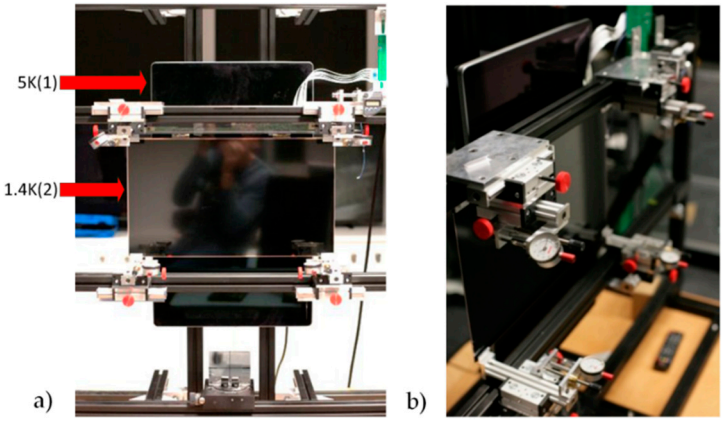

Figure 8. Demonstrator, with 90° crossed display panel, mounted to a metal frame with calibration fixtures. (**a**) frontal view and (**b**) lateral view with details.

The measured luminance losses of the system (see Table 2) are approximately 91% and are caused by the geometric properties of the display pixels and by the spectral properties of the arrangement. The question is how this value can be improved. Therefore, we have to understand the conditions that reduce this value.

Table 2. Luminance of single displays and the demonstrator with white and prime-color (red, green and blue).

Spectral Luminance	Display 1 (5 K)	Display 2 (1.4 K) *	Demonstrator, Displays 1 + 2
White Pixel Luminance	214 cd/m²	158 cd/m²	18.6 cd/m²
Red Pixel Luminance	56 cd/m²	32 cd/m²	5.3 cd/m²
Green Pixel Luminance	146 cd/m²	109 cd/m²	9.8 cd/m²
Blue Pixel Luminance	12 cd/m²	17 cd/m²	0.9 cd/m²

* Values measured with the display backlight (the backlight was removed in the mock-up assembly).

Figure 9 shows the geometric differences between the idealized and real apertures of the pixel designs, in Figure 9a for the image display and in Figure 9b for the color barriers.

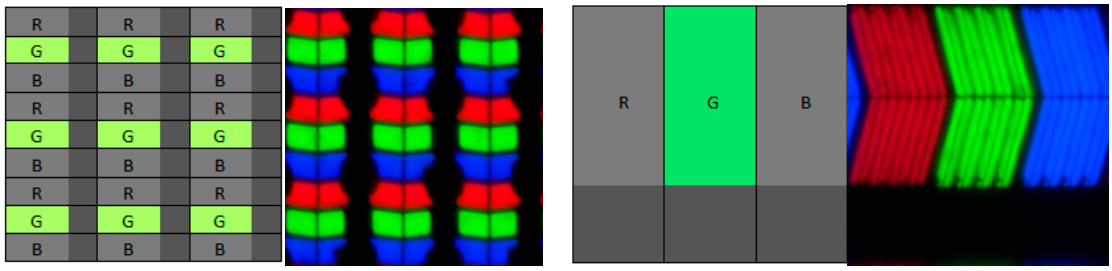

Figure 9. Comparison of idealized subpixel structures (only green glows) on the left with the real subpixel structures on the right. (**a**) Display 1 (image display) and (**b**) Display 2 (color barrier).

Due to the non-transparent gaps between the pixels, the light intensity emitted by the subpixels will be reduced by approximately 1/3. The idealized gap structure was simulated by the in-house software; the luminance profiles in Figure 5 were calculated based on this model. Furthermore, the crossed arrangement of displays and the proportion of pixels cause an additional 2/3 reduction of the light intensity. The geometrical reduction factor results in approximately 2/9 or 22% transmission of the source intensity of Display 1.

3.2. Spectral, Luminance and Crosstalk Measurements

It is generally known that the visible crosstalk is an overlay [22–24] by optical crosstalk due to the non-ideal spectral separation of the primary colors and electrical crosstalk due to the electrical coupling between the subpixels in the matrix. In our 3D display arrangement, the individual spectral fractions of prime-colors of both displays clearly differ. This leads to a visible color crosstalk and a reduction of light transmission for this demonstrator arrangement with Displays 1 + 2. In Table 2, the measured luminance of prime-colors of Displays 1 + 2 does not add up to the measured white-luminance.

In Figure 10, the measured values of the whole display demonstrator are indicated by the left and the right graphs. Differences in the spectral distributions of Displays 1 and 2 reduce the intensity from 22% down to 12%. Thus, the combination of geometrical and spectral properties determines a transmission loss of approximately 88%. The measurement results of the single color arrangements will be explained by one example; the green-green combination with max. 10 cd/m². The white-green combination shows a reasonable amount of red intensity in the transmitted green area from 570–620 nm. This is caused by the broad green emission and filter characteristics of Display 2. The measured intensity transmitted through the demonstrator corresponds to only 7% of source luminance depicted in the green filled area in the right part of Figure 10. An explanation for the remaining 5% difference can be given by absorption losses and stray light in the polarizer, glass and filter layers of Display 2.

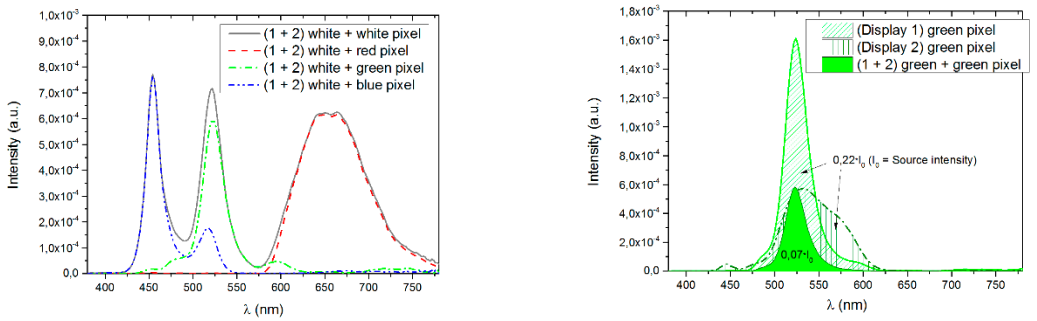

Figure 10. Left: Display 1 with white spectrum and 90° tilted Display 2 with single prime-colors, visible crosstalk of blue in green; **right:** spectral intensity of the green color primaries from both panels.

To analyze the color filter design for the two view setup of Section 2 shown in Figure 4, the measurement and the simulation use the same test pattern and parameter sets. The pixel pitches are input parameters from Table 1. From Figure 9, the pixel areas were used for the calculation of the luminance distribution. For their analysis, the first test pattern used only one emitting green column per stripe image. In addition, the measured green luminance of 146 cd/m² for Display 1 was used as the simulation input. The crosstalk values were determined from the angle-dependent luminance profile.

The measured luminance distributions for the green single-columns (views 1 and 2, respectively left and right) are shown in Figure 11.

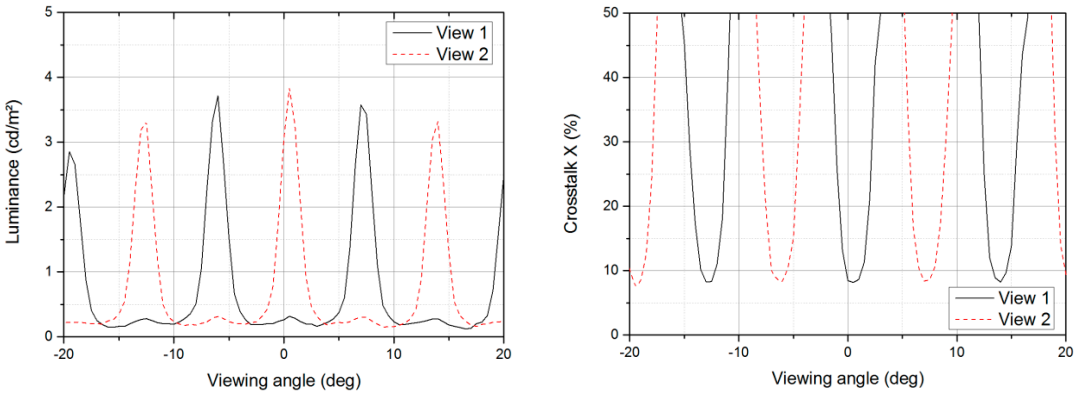

Figure 11. Left: experimental measured luminance for views 1 and 2; **Right**: crosstalk green for views 1 and 2, one channel green/one channel black.

Besides the main peaks, there are smaller peaks visible for the two views, where the minimum luminance is 0.2–0.3 cd/m². The measured ground level of about 0.2 cd/m² cannot be explained by the black level of the display. Its value of about 0.05 cd/m² was determined in a control measurement. The observed increase of the lower luminance values is mainly caused by electrical and optical crosstalk. In the process of electrical addressing, black subpixels with low intensity are slightly stimulated [25].

The causes for the different kinds of crosstalk cannot be precisely separated by measurement technology. Therefore, it is complex to consider this in the simulation [26]. Taking this into account, we have defined a parameter for the spectral residual light components that occur as a result of the unwanted electrical crosstalk. That parameter is valid for the complete display assembly. It is weighting the visible area fractions of the subpixels [17] and the maximum luminance of the subpixel colors in the simulation. These corrected values will be part of the calculation of luminance in the subpixel positions. Thus, we defined further parameters of the spectral transmission for every of the six subpixel positions of the stripe image. With these parameters, we take into account the differences in color intensity of the demonstrator. They are caused by the spectral profile of the backlight and the special filter characteristics of the primaries.

Figure 12 shows the simulated and measured graphs of luminance and their crosstalk profiles. The new defined parameters were careful modified to adapt them to the original measurement graph. The difference in luminance between simulation and measurement is caused by the spectral intensity losses of our mock-up arrangement. However, the simulation of the measurement is well approximated for the green image parts. The spectral transmission was estimated to about 55% by integration of the overlapping area under the primary peaks of Displays 1 and 2; see Figure 10. The low maximum transmission leads to crosstalk values round 8% for a one-channel-arrangement and a min. of 15% for a three-channel arrangement in Figure 13.

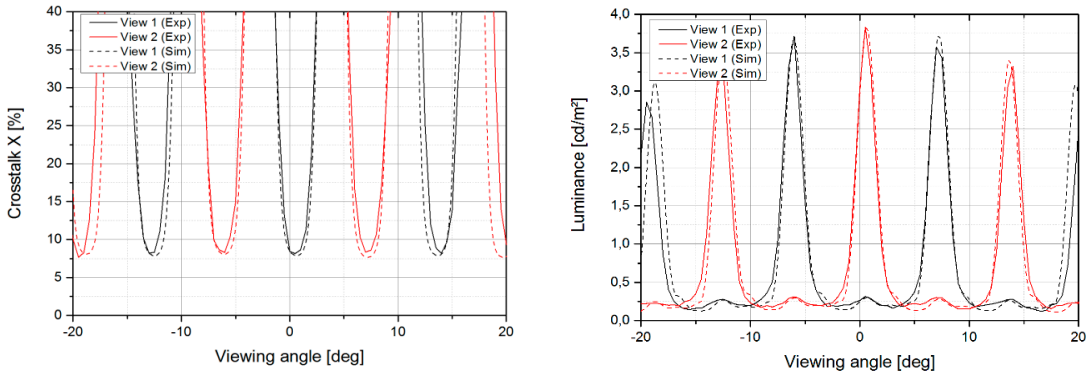

Figure 12. Left: simulated and experimental measured luminance for views 1 and 2; **right**: crosstalk of green between views 1 and 2, one channel green/one channel black.

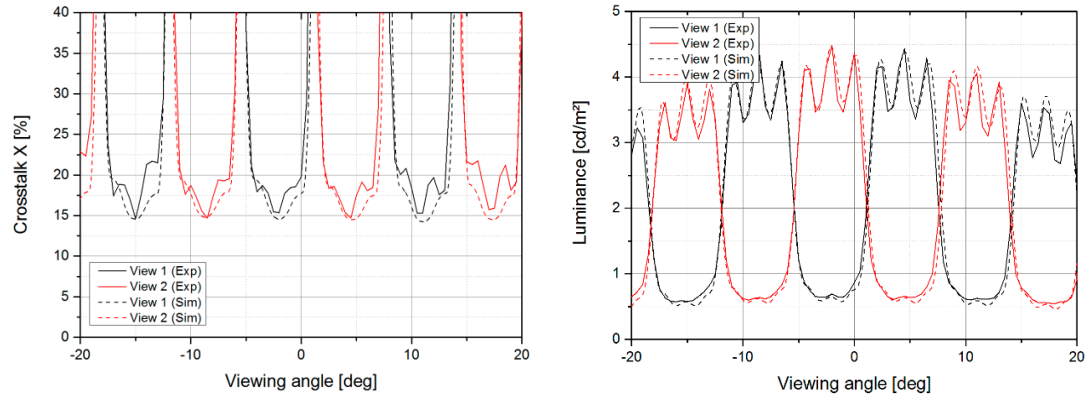

Figure 13. Left: simulated and experimental measured luminance for views 1 and 2; **right**: crosstalk of green between views 1 and 2, three channels green/three channels black

Furthermore, in Figure 13, the measurements and simulation results with three-times wider channels (three neighboring sub-pixel columns are bright) show a three-fold sub-structuring of luminance peaks instead of the expected luminance plateaus. Actually, the reason for this sub-structuring can be determined by the simulation software. It is caused by the structure of subpixels, shown in Figure 9. The palmate sub-structure in the graphs of Figure 13 is dependent on the size and alignment of the gaps between the subpixels.

The proposed geometric design approach was verified by the experiment, but the 3D display demonstrator also shows an inadequate amount of color filter crosstalk. It has been demonstrated that a very specialized display design is necessary when a fast switchable barrier with high aperture, high transmission and excellent color separation has to be planned. Therefore, a novel color filter based on common nematic liquid crystals (NLC) was developed and investigated.

3.3. Evaluation of Novel Fast Tunable Interference Color Filter

The switching times of the electric field-driven reorientation of NLCs are given by Equations (6) and (7), respectively.

$$t_{\text{on}} = \frac{\gamma_1 d^2}{\epsilon_0 |\Delta\epsilon| \left(u^2 - u_{\text{th}}^2\right)} \text{ with } u_{\text{th}} = \pi \sqrt{\frac{K_{11}}{\epsilon_0 |\Delta\epsilon|}} \tag{6}$$

$$t_{\text{off}} = \frac{\gamma_1 d^2}{(\pi^2 K_{11})} \tag{7}$$

Here, γ_1 is the NLC rotational viscosity, d is the NLC layer thickness, ϵ_0 is the free space permittivity, $\Delta\epsilon$ is the anisotropy of the dielectric constant of the NLC, K_{11} is the NLC splay elastic

constant, U is the applied voltage and U_{th} is the NLC threshold voltage. Both t_{on} and t_{off} are directly proportional to the square of the layer thickness. Accordingly, the Lyot filter stage with the thickest NLC layer limits the switching time of the entire stack. Its usual large thickness leads to relatively long switching times ranging from tens to hundreds of milliseconds. The tunable NLC Fabry–Pérot filters have the potential to switch significantly faster. They consist of a single cavity sandwiched between mirrors and electrodes. Their simple structure enables one to minimize the NLC layer thickness and thus to improve the switching time. As shown by Equation (8), a decreasing cavity thickness also results in an increase of the free spectral range (FSR), which stands for the distance between two successive transmission peaks.

$$\mathrm{FSR} = \frac{2nd\cos\Theta}{m(m+1)} \text{ with } m = \frac{2nd\cos\Theta}{\lambda} \quad (8)$$

Here, n is the refractive index; Θ is the angle of incident; m is the interference order; d is the cavity thickness; and λ is the resonance wavelength. However, the conventional spacer technologies used for the construction of the reported examples limit the minimum thickness of the NLC layer to about 2 µm [27]. At this layer thickness, the electro-optical properties of NLCs are still not optimally utilized, and the small FSR limits the applicability in the visible range. Consequently, no example of a fast switchable interference filter for the visible range has yet been reported.

In this paper, we present a design concept and three examples of a fast tunable NLC Fabry–Pérot interference filter operating in the visible range. It consists of a sub-micrometer-thick NLC layer embedded in a matched filter design. The electro-optical properties of the interference filters were characterized by Vis-spectroscopic and switching time measurements as a function of the applied voltage. The obtained data prove the design concept of the fast tunable color filters. The basic structure of the designed electrically-tunable NLC Fabry–Pérot color filters is shown in (Figure 14). The devices were manufactured by assembling two half cells followed by filling the resulting cell gap with an NLC. One of the half cells consists of a glass plate successively coated with ITO, a dielectric mirror and a photo-structured alignment layer [28,29] and the other one of a glass plate successively coated with ITO, a dielectric mirror and patterned spacer. The key element of the electrically-tunable color filter (Figure 14) is a sub-micrometer-thick NLC layer, which is homogeneously planar orientated by the adjacent alignment layer. The NLC and alignment layer fill the cavity between two dielectric mirrors. In the field-free state, the NLC layer is birefringent.

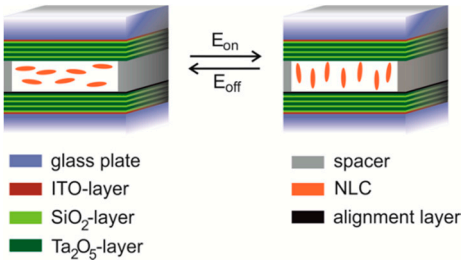

Figure 14. Overview of the basic configuration of the nematic liquid crystal (NLC) Fabry–Pérot color filter and the principle of the switching in an electric field E.

Each resonance peak is split into two mutually perpendicular linearly-polarized peaks; one polarized along the long and the other polarized along the short molecular axis of the NLC. The distance between the two peaks is determined by the birefringence of the NLC-alignment layer stack. If a voltage above U_{th} is applied in the direction of the layer normal, a reorientation of the NLC into a homeotropic alignment takes place (Figure 14). This results in the disappearance of the peak splitting. For thin cavities of the Fabry–Pérot filter, the distributed reflection of the dielectric mirrors has to be taken into account to calculate the positions of the resonance peaks [30]. This effect leads to a reduction of the peak distances with decreasing cavity thickness and, thus, to a reduction of the shifting range. As a compromise of an optimized shifting range and a sufficient FSR in the visible range, the 2λ resonance peak was selected to operate the color filters. This corresponds to an optical

path length of 800–1600 nm. [31] Taking the refractive index of the NLC into account being typically in the range of about 1.5–1.75, cavity thicknesses of about 0.5–1 μm are required.

For the experimental verification of the electrically-tunable color filter performance, three test devices were constructed, which operate in the red, green or blue regions of the visible range. The specific device parameters are listed in Table 3.

Spacer thickness and the dielectric mirror of each device were adapted to the desired spectral operating range. Patterned sub-micrometer-thick spacers with a specific thickness were manufactured by a coating process in which SiO_2 was sputtered through a shadow mask on top of the respective substrate. The spacer thickness thus could be controlled with an accuracy of 1 nm.

Table 3. Cell parameters of the devices: mirror design and layer thicknesses.

Device	Mirror Design [(1)]	Mirror Materials SiO_2/Ta_2O_5	Electrode ITO (indium tin oxide)	Spacer SiO_2
I	$(HL)^4$ H	106 nm/73 nm	40 nm	817 nm
II	$(HL)^4$ H	96 nm/64 nm	40 nm	753 nm
III	$(HL)^4$ H	76 nm/51 nm	40 nm	583 nm

[(1)] The layer design is denoted by $(HL)^m$ *X* in which (HL) stands for the unit structure consisting of a layer *H* with a high and a layer *L* with a low refractive index; both layers with an optical thickness of a quarter of the design wavelength; *m* stands for the number of periods of the multilayer stack, and *X* = *H* or *L* for the layer on top of the substrate (here, the layer adjacent to the alignment layer or to the NLC layer of the devices).

The optical properties of the devices were characterized by Vis-spectroscopic measurements. As an example, the spectra of Device I in the off-state and on-state are displayed in Figure 15. In the off-state, a split of the 2λ resonance peak into two equally-sized peaks is observed. Both peaks are mutually perpendicular linearly-polarized as displayed when inserting a linear polarizer into the path of the beam of the spectrometer. By rotating this polarizer, one or the other peak can be completely eliminated while the other reaches maximum intensity.

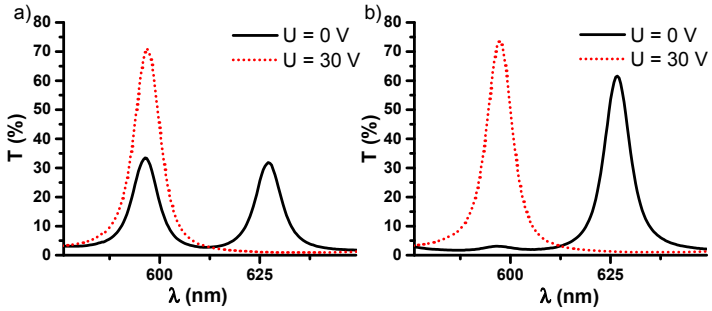

Figure 15. Transmission of Device I in the off-state (—) and in the on-state (···) measured with non-polarized (**a**) and with linear polarized (**b**) incident light.

This result indicates a homogeneously planar orientation of the NLC. One peak occurs at λ_{max} = 596 nm, corresponding to the refractive index along the short molecular axis of the NLC (n_o), and the other at λ_{max} = 627 nm, corresponding to the refractive index along the long molecular axis of the NLC (n_e). Applying a DC voltage of 30 V between the ITO layers leads to a switching into the on-state and, thus, to the disappearing of the resonance peak splitting. The peak at λ_{max} = 596 nm remains unaffected by the electric field, while at the same time, the peak at λ_{max} = 627 nm shifts to λ_{max} = 597 nm, where both peaks overlap. These findings indicate a homeotropic alignment of the NLC. By switching off the electric field, the NLC returns to the planar orientation, and again, each resonance peak splits into two equally-sized peaks. In summary, the 2λ resonance peaks of Device I can be reversibly shifted through an applied electric field by 30 nm within the red region of the visible range. Switching time measurements reveal that the peak shift in both directions can appear in the millisecond regime or even faster. It responds to an applied DC voltage of 30 V for t_{on} = 0.11 ms, and t_{off} = 1.1 ms was obtained. These switching times are much faster than reported for NLC Lyot

filter stacks or NLC Fabry–Pérot filters with cavity thicknesses of several μm being in the range of tens to hundreds of milliseconds [32]. Similar electro-optical properties were obtained for Devices II and III. Peak positions (λ_{max}) of the 2λ resonance peaks, as well as the t_{on} and t_{off} switching times are listed in Table 4.

Table 4. Measured electro-optical properties of the devices for red, green and blue transmission.

Device	Switching On-State	Switching Off-State		Switching Times (U = 30 V)	
No.	λ_{max} of the 2λ Resonance Peak	λ_{max} of the 2λ Resonance Peaks		t_{on}	t_{off}
I	597 nm	596 nm	627 nm	0.11 ms	1.1 ms
II	545 nm	544 nm	576 nm	0.11 ms	1.1 ms
III	479 nm	479 nm	501 nm	0.10 ms	1.1 ms

As can be seen, the performed variation of the cavity thickness of the devices shifts the positions of their resonance frequencies without significantly affecting their operation range and switching times. Whereas Device I operates in the red region, Devices II and III operate in the green or blue region of the visible range, respectively.

Illuminating the devices with a monochromatic backlight whose wavelength matches the device specific peak position of the electrically-tunable 2λ resonance peak in the off-state, the devices can operate as a fast switchable barrier filter. This operation mode is displayed in Figure 16. In the off-state, the backlight can pass the devices, and thus, they shine red (Device I), green (Device II) or blue (Device III). Switching the devices from the off-state into the on-state shifts their 2λ resonance peaks out of the spectrum of the backlight. Accordingly, the devices appear dark (see the on-state in Figure 16). The same effect could be realized by using a narrowband LED emitting at λ_{max} = 574 nm with a full width at half maximum of 11 nm as the backlight for Device II.

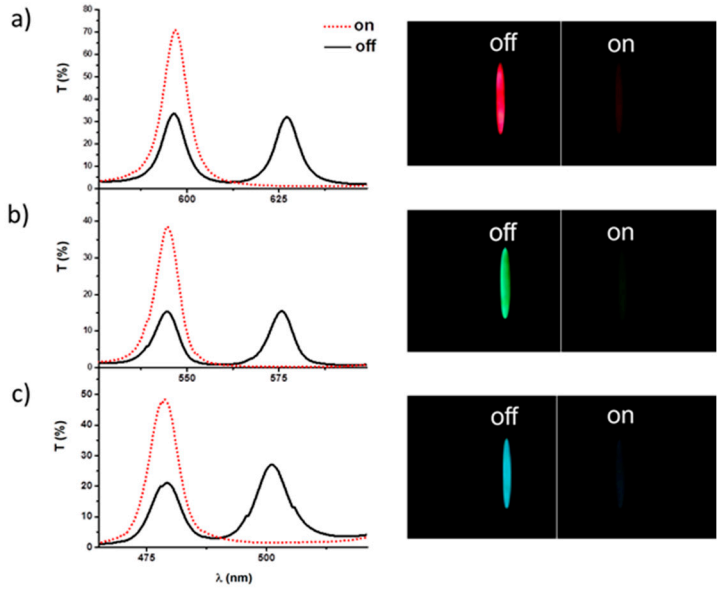

Figure 16. Transmission and visual appearance for the devices dedicated to a monochromatic incident light for red (**a**), green (**b**) and blue (**c**).

Again, the device operates as a fast switchable barrier filter, and a green to dark switching is observed. Although the anisotropy of the birefringence of the used NLC is rather small (Δn = 0.11) compared to high birefringence NLC (Δn up to 0.7) [33,34], the resulting operation range of about 30 nm is already large enough for the demonstrated barrier filter function.

Illuminating the devices with linear polarized light enables switching the wavelength of the transmitted light. This operation mode of Device I is displayed in Figure 15b. In this mode, the polarization direction of the incident light is aligned in the direction of the long molecular axis of the

NLC, and thus, only the electrically-switchable transmittance peak appears in the off-state. By applying an electric field, the transmittance peak is shifted by about 30 nm. This shift takes place within the free spectral range of the off-state.

The performance of the presented filter design depends to a large extent on the choice of the NLC. For the present study, a eutectic mixture of NLC compounds known to provide low γ_1 and low U_{th} was used [35]. The design of the NLC with a view toward specific applications clearly bears high potential to improve the required NLC Fabry–Pérot filter properties.

For example, the incorporation of high birefringence NLC should lead to strongly increased operating ranges. Another potential for improvement comes from the technological side. Further decrease of the cavity thickness would result in faster switching times and increased FSR as displayed by Equations (6)–(8). Such investigations are currently underway.

4. Discussion

A time-sequential working spatially-multiplexed autostereoscopic 3D display concept consisting of a fast switchable RGB-color filter array could be presented. The assembling of such a large array with wavelength-selective filters used as the image splitter barrier has been simulated in interaction with a color display matrix. As an outstanding result, such a barrier emits the light from a display over a larger active area than common autostereoscopic barrier displays. The separation of equally-colored subpixel columns, which are separated by two differently-colored columns, produces in the simulation excellent crosstalk suppression.

According to progress in the project, no large-scaled sample of the described switchable color barriers was available for the experimental verification of the arrangement. For that reason, commercial display components had to be used. Because of the low switching speed of these components and the non-synchrony address directions (one display is 90° rotated), the measurements and correspondingly the simulations of this system were carried out on static switching states. The search for suitable components yielded only a single display combination that fulfilled the requirements for suitable resolutions, pixel pitches and polarizer alignment. The color subpixels of both of these display components are small and exhibit unfavorable geometric and optical properties, which greatly reduce the brightness and cause an inadmissible crosstalk. Both components have been combined in a mock-up by replacing the backlight of the barrier display in front of the assembly. Using a green test pattern, it could be shown on the display mock-up that the introduced assembling of the display and color barrier array creates an autostereoscopic display image in every switching state. The documentation and analysis of the image properties was only possible by means of optical measurement technology. The influence of the gaps in display cells and in the barrier stripes was detected and examined with the help of the simulation.

It was not possible to separate the kinds of crosstalk at the measurements of the demonstrator. However, the influence of electrical and optical crosstalk could be simulated with a simulation approach. In that way, it was possible to reproduce the luminance curve sufficiently well, due to the used parameters with different influences on the luminance curve. The causes of the crosstalk (optial & electrical) in the static image could thus be assigned unambiguously by the simulation. The temporal superimposition of the 3D representations generated in the successive switching stages led to the desired resolution improvement. Dynamic switching processes in the display and barrier increase the optical crosstalk. Further research is necessary to take this into consideration in the simulation.

However, the hitherto performed investigations show that time-sequential wavelength-separated 3D displays need special designs of the LC-matrix, which strongly reduce the electrical crosstalk. The traditional color filter cells used for commercial nematic displays have inadmissibly high optical leakages and an insufficient switching speed for their application in time-sequential wavelength-selective autostereoscopic displays. Therefore, other, extremely fast switchable filter designs with excellent color separation have to be used in the display and barrier.

In this paper, we present a design concept of a fast tunable NLC Fabry–Pérot interference filter cell operating in the visible range. It consists of a sub-micrometer-thick NLC layer embedded in a

matched filter design. An experimental proof of the feasibility of NLC Fabry–Pérot filters for the construction of the millisecond regime tunable color filters is given. Reducing the cavity thickness of the NLC Fabry–Pérot filter to the sub-micrometer region improved the switching times, and an extension of the FSR in the visible range was achieved. The usable operation range of the presented filters amounts to about 30 nm. In combination with a matching of monochromatic or narrowband backlight, the filter can operate as a barrier filter switching between a transparent and a non-transparent state. Illuminated with linear polarized light, the filter enables tuning the central wavelength of the narrowband transmitted light.

The results obtained in the simulation and in the practical tests showed that novel application fields can be developed with very fast switchable color filters. The possible application fields of this technology in 3D display constructions are not only the central perspective barrier designs presented here for two-view and multiview 3D displays. Rather, the design rules shown by us in [6] also permit the application of the presented switchable, wavelength-based selection barrier display arrangement to parallel and divergent radiating 3D displays. The good color separation of Fabry–Perot cells or the alternative of filter cells with bandpass characteristics can be used in multi-layered displays (staked displays) [36–39]. This would cause a significant crosstalk reduction.

In the case of the time-consistent spectacle-free 3D representation, further investigations are necessary in order to realize large-format, wavelength-selective filter arrays. This relates, on the one hand, to improved, rapidly-switchable filter cells with bandpass characteristics that can be viewed from a large angular range. On the other hand, further work is also necessary in the matrix display drive in order to enable a good image separation of spatially-multiplexed 3D displays. Today's displays impress with their high resolution. In the proposed design, an HD-resolution 3D display requires more than 6000 switchable color filter strips with nematic layers in the sub-micrometer range. The necessary technology for large area components is not yet available.

5. Methods and Materials

The time-sequential autostereoscopic visualization with a wavelength-selective barrier and display is one of the computational display technologies, in which a number of display layers (1 ... *Q*) is controlled by means of adaptive image processing algorithms [39]. The temporal sequence of differently-directed image information increases the visible image resolution. The simultaneous use of all primary colors of the display for the wavelength selection avoids the color breakup [40] known from color-sequential display modes [41].

For the theoretical analysis of such complex assembles, an in-house simulation tool for flat spatial multiplexed 3D displays, developed by Fraunhofer HHI [1], was modified with a geometrically-optical model of wavelength-selective barriers. It has been used to simulate several aspects of spatially-multiplexed autostereoscopic displays [17] and for the automatic evaluation of 3D display designs [18].

The tool allows you to simulate the properties of the display and the image splitter. For this purpose, selected light beams emanating from the display elements are calculated on the basis of the geometrical optics. Radiated light quantities, otherwise measured by means of a spectrometer, are calculated by integrating the corresponding intensities in the visible display areas depending on the luminance values. In order to examine the image separation, the subpixel surfaces are provided with different, interlaced image information in the simulation as in the real system. The image information of the illuminating subpixel is therefore also the basis of each calculated light beam. A simulation of the switching transitions has been dispensed with. Thus, only static switching states are considered in order to be able to evaluate the basic functioning of the arrangement. The tool was implemented on a PC system (ASUS ROG G20AJ-DE045S, ASUSTeK Computer Inc., Taipeh, Taiwan). The layouts of subpixels and the wavelength-selective image splitter were described in modeling of the idealized form. This means that the subpixels and filter strips were executed as rectangular surfaces. On the one hand, the graphics processor unit based rendering did enable displaying the path of rays by the laws of geometrical optics. On the other hand, it was possible to calculate the optical result, visible from the eye-position of an observer. For the necessary

calculations, a graphics controller GEFORCE GTX 980 (manufacture EVGA Corp., Brea, CA, USA) based on NVIDIA 980 GTX (Nvidia Corp., Santa Clara, CA, USA) was applied. The algorithm used DirectX11 to render the model construction and used OpenCL to evaluate a selected design choice.

The large-area 3D display mock-up was realized on a test carrier from item™-profiles and micrometer drives. The content display (Display 1) was a monitor UP2715K from DELL Technologies (Round Rock, TX, USA), and for the color filter barrier, an RGB matrix panel LC216EXN from LG (Display 2) (LG Display, SeoulSouth, Korea) was used. For illumination purposes for Display 1, the complete backlight of Display 2 was removed. For the control of the display combination, a PC with a graphics controller based on NVidia 980 GTX was applied. The subpixel pattern of the used displays was documented by a Wild-Leica stereo-microscope MZ3 (Leica Microsystems, Wetzlar, Germany) with 80-times magnification. The luminance measurements were taken by a PR-680 radio-spectrometer from Photo Research Inc. (Syracuse, NY, USA) with a goniometrical rotary stage RF1 from isel Germany AG (Eiterfeld, Germany) and a stepper motor controlled by a PC. The measuring instrument was arranged at a one-meter distance. It registered the light in a measuring diameter of 17.4 mm.

A eutectic mixture of 3,4-difluoro-4′-(4-propyl-cyclohexyl)biphenyl, 3,4-difluoro-4′-(4-pentyl-cyclohexyl)biphenyl and 3,4,5-trifluoro-4′-(4-pentyl-cyclohexyl)biphenyl was used as the electrically-tunable NLC resonator medium. The mixture exhibits a nematic phase in between 17.3 °C (melting point) and 67.3 °C (nematic to isotropic transition). The refractive indices of the NLC at room temperature are n_o = 1.55 and n_e = 1.66. Simulations of the optical properties of various filter designs were carried out by using the program OptiLayer from OptiLayer GmbH (Garching, Germany). The NLC Fabry–Pérot color filters were manufactured under clean-room conditions. The two half cells were plane-parallel assembled in analogy to the conventional LCD manufacturing technology [42,43].

Switching times were measured optically at room temperature. The devices were mounted in normal transmission geometry between crossed polarizers on an OLYMPUS BH-2 microscope (Olympus Corp., Tokyo, Japan) fitted with a H10722-01 photomultiplier tube (Hamamatsu Photonics, Hamamatsu-shi Shizuoka, Japan) and an digital storage oscilloscope DSO-X-3024A (Agilent Technologies, Santa Clara, CA, USA). Then, the device was rotated within the plane to the position of maximum transmittance. Switching times were defined as the 90% to 10% or 10% to 90% transmission changes in response to a pulsed DC voltage. Spectroscopic measurements were carried out by using an USB 2000 + spectrometer (Ocean Optics Inc., Dunedin, FL, USA). All measurements were performed at room temperature. A Jasco V-670 spectrometer (JASCO Germany GmbH, Gross-Umstadt, Germany) was used to generate monochromatic light of specified wavelength and a Toshiba TLGU1008 LED (Toshiba Lighting and Technology, Tokio, Japan) to generate a narrowband light with a central wavelength of 574 nm. These light sources were applied as backlights for the demonstration of the barrier filter function of the manufactured NLC Fabry–Pérot color filters.

Acknowledgments: Financial support by Fraunhofer-Gesellschaft, München (Project Number 600 334), is gratefully acknowledged.

Author Contributions: R.d.l.B. led the project and wrote the paper together with R.B. and S.B. made the simulations. S.J. analyzed the simulation result. M.K. programmed the simulation tools. R.B. made optical measurements and analyzed them. D.L. and C.R. made the cell design. H.B., M.G. and J.F. contributed reagents/materials/analysis. A.S., P.F. and G.S. optimized the labor methodology. B.D. created the laboratory technique and test procedures.

Conflicts of Interest: The authors declare no conflict of interest.

References

1. Urey, H.; Chellappan, V.K.; Erden, E.; Surman, P. State of the Art in Stereoscopic and Autostereoscopic Displays. *Proc. IEEE* **2011**, *99*, 540–555.
2. ISO. *Ergonomics of Human-System Interaction—Part 331: Optical Characteristics of Autostereoscopic Display*; ISO TR-9241-331:2011(E), Technical Report; ISO: Geneva, Switzerland, 2011.

3. Zhang, Q.; Kakeya, H. Time-Division Quadplexing Parallax Barrier Employing RGB Slits. *JDT* **2016**, 12, 626–631.
4. Zhang, Q.; Kakeya, H. Time-division multiplexing parallax barrier based on primary colors. *SPIE* **2014**, *9011*, doi:10.1117/12.2042313.
5. Bartmann, R.; Kuhlmey, M.; Netzbandt, R.; de la Barré, R. Simulation of autostereoscopic displays by geometrical ray tracing and implication of optical effects. In Proceedings of the 3DTV-Conference: The True Vision—Capture, Transmission and Display of 3D Video (3DTV-CON), Budapest, Hungary, 2–4 July 2014.
6. De la Barré, R.; Hopf, K.; Jurk, S.; Leiner, U. TRANSFORMERS–Autostereoscopic Displays Running in Different 3D Operating Modes. *SID Symp. Dig. Tech. Pap.* **2011**, *42*, 452–455.
7. Jurk, S.; Kuhlmey, M.; de la Barré, R. A new type of multiview display, IS&T/SPIE Electronic Imaging 2015. In Proceedings of the Stereoscopic Displays and Applications XXVI, San Francisco, CA, USA, 9–11 February 2015.
8. Woltman, S.J.; Jay, G.D.; Crawford, G.P. Liquid-crystal materials find a new order in biomedical applications. *Nat. Mater.* **2007**, *6*, 929–938.
9. Gat, N. Imaging spectroscopy using tunable filters: A review. *Proc. SPIE* **2000**, *4056*, doi:10.1117/12.381686.
10. Beeckman, J.; Neyts, K.; Vanbrabant, P.J.M. Liquid-crystal photonic applications. *Opt. Eng.* **2011**, *50*, 081202.
11. Patel, J.S.; Saifi, M.A.; Berreman, D.W.; Andreadakis, C.L.N.; Lee, S.D. Electrically tunable optical filter for infrared wavelength using liquid crystals in a Fabry-Pérot étalon. *Appl. Phys. Lett.* **1990**, *57*, 1718–1720.
12. Abdulhalim, I. Non-display bio-optic applications of liquid crystals. *Liq. Cryst. Today* **2011**, *20*, 44–60.
13. Kong, Y.; Yang, G.; Huang, X. Multiple-stage liquid crystal tuned filter. *Opt.-Int. J. Light Electron Opt.* **2011**, *122*, 1723–1729.
14. Hamdi, R.; et al. Optical bandpass Lyot filter with tunable bandwidth. In Proceedings of the 19th International Conference on Telecommunications (ICT), Jounieh, Lebanon, 23–25 April 2012.
15. Okoshi, T. *Three-Dimensional Imaging Techniques*; Academic Press: New York, NY, USA; San Francisco, CA, USA; London, UK, 1976.
16. Schmidt, A.; Grasnick, A. Multi-viewpoint Autostereoscopic Displays from 4D-Vision. *SPIE* **2002**, *4660*, 216–217.
17. Bartmann, R.; Kuhlmey, M.; Netzbandt, R.; de la Barré, R. Validation of subpixel area based simulation for autostereoscopic displays with parallax barriers. In Proceedings of the International Conference on 3D Imaging (IC3D), Liège, Belgium, 9–10 December 2014.
18. Kuhlmey. M.; Jurk, S.; Duckstein, B.; de la Barré, R. Automated simulation and evaluation of autostereoscopic multiview 3D display designs by time-sequential and wavelength-selective filter barrier, SPIE Optical Systems Design 2015. *Comput. Opt. Proc. SPIE* **2015**, *9630*, doi:10.1117/12.2191339.
19. Jurk, S.; Kuhlmey, M.; Bartmann, R. ; Duckstein, B.; de la Barré, R. Autostereoscopic display concept with time-sequential wavelength-selective filter-barrier. *Proc. SPIE Adv. Disp. Technol. VI* **2016**, *9770*, doi:10.1117/12.2214344.
20. Jurk, S.; de la Barré, R. A new Tracking Approach for XYZ-User-Adaption of Stereoscopic Content. In Proceedings of the Electronic Displays Conference, Nuremberg, Germany, 25–27 February 2014.
21. de la Barré, R.; Jurk, S. Improvements of aid free 3D Presentation. In Proceedings of the Electronic Displays Conference, Nuremberg, Germany, 2–3 March 2011.
22. Tamura, N.; Tsumura, N.; Miyake, Y. Masking Model for accurate Colorimetric characterization of LCD. In Proceedings of the 10th IS&T/SID Color Imaging Conference 2002, Scottsdale, Arizona, USA, 12–15 November 2002; pp. 312–316.
23. Yoshida, Y.; Yamamoto, Y. Color Calibration of LCDs. In Proceedings of the 10th Color Imaging Conference, Scottsdale, AZ, USA, 12–15 November 2002; pp. 303–311.
24. Becker, M. Metrology Issues for LCD-TV, pp. 1–11, © Display-Metrology&Systems 2005. Available online: http://www.display-messtechnik.de/fileadmin/template/main/docs/metrology4lcd-tv.pdf (accessed on 10 December 2016).
25. Mantiuk, R.; Daly, S.; Kerofsky, L. The luminance of pure black: Exploring the effect of surround, in the context of electronic displays.In Proceedings of the Human Vision and Electronic Imaging XXI, IS&T/SPIE's Symposium on Electronic Imaging, San Jose, CA, USA, 18–21 January 2010; pp. 7527–7531.
26. Wen, S.; Wu, R. Two-Primary Crosstalk Model for Characterizing Liquid Crystal Displays. *Res. Appl. Wiley Period.* **2006**, *31*, 102–108.

27. Isaacs, S.; Placido, F.; Abdulhalim, I. Investigation of liquid crystal Fabry–Pérot tunable filters: Design, fabrication, and polarization independence. *Appl. Opt.* **2014**, *53*, H91–H101.
28. Schadt, M.; Seiberle, H.; Schuster, A. Optical patterning of multi-domain liquid-crystal. *Nature* **1996**, *381*, 212–215.
29. Neill, M.O.; Kelly, S.M. Photoinduced surface alignment for liquid crystal displays. *J. Phys. D Appl. Phys.* **2000**, *33*, R67.
30. Garmire, E. Theory of quarter-wave-stack dielectric mirrors used in a thin Fabry-Pérot filter. *Appl. Opt.* **2003**, *42*, 5442–5449.
31. Seeboth, A.; Lötzsch, D.; Rabe, C.; Frach, P.; Gittner, M.; Bartzsch, H.; de la Barré, R.; Bartmann, R.; Vergöhl, M.; Bruns, S.; et al. Electrically Controlled Interference Color Filter. Patent WO 2016113051A1, 21 July 2016.
32. Hirabayashi, K.; Tsuda, H.; Kurokawa, T. Tunable liquid-crystal Fabry-Pérot interferometer filter for wavelength-division multiplexing communication systems. *J. Lightwave Technol.* **1993**, *11*, 2033–2043.
33. Dąbrowski, R.; Kula, P.; Herman, J. High Birefringence Liquid Crystals. *Crystals* **2013**, *3*, 443–482.
34. Gauza, S.; Kula, P.; Dabrowski, R.; Sasnouski, G.; Lapanik, V. Review Paper: High Optical Anisotropy Nematic Single Compounds and Mixtures. *Trans. Electr. Electron. Mater*. **2012**, *13*, 2–5.
35. Hird, M. Fluorinated liquid crystals—Properties and applications. *Chem. Soc. Rev.* **2007**, *36*, 2070–2095.
36. Masia, B.; Wetzstein, G.; Didyk, P.; Gutierrez, D. A Survey of Computational Displays. Pushing the Boundaries of Optics, Computation and Perception. *Comput. Graph.* **2013**, 37, 1012–1038.
37. Wetzstein, G; Lanman, D.; Gutierrez, D.; Hirsch, M. Computational Displays. In *SIGGRAPH* 2012 course; ACM: New York, NY, USA, 2012.
38. Wetzstein, G; Lanman, D.; Hirsch, M.; Raskar, R. Tensor Displays: Compressive Light Field Synthesis using Multilayer Displays with Directional Backlighting. *ACM Trans. Graph.* **2012**, *31*, 80.
39. Heide, F.; Wetzstein, G.; Raskar, R.; Heidrich. W. Adaptive Image Synthesis for Compressive Displays. *SIGGRAPH. ACM Trans. Graph*. **2013**, *32*, 132.
40. Johnson, P.V.; Kim, J.; Banks, M.S. The visibility of color breakup and a means to reduce it. *J. Vis.* **2014**, *14*, 10.
41. Baron, P. C. . Saccadic color breakup in field sequential color displays: An overview. In Proceedings of the Americas Display Engineering and Applications Conference (ADEAC06), Atlanta, Georgia, USA, 24–26 October 2006.
42. Seeboth, A. Orientation layers for liquid crystals in liquid crystal displays. *Displays* **1999**, *20*, 131–136.
43. Seeboth, A. Electro-optical behavior of polymer-dispersed liquid crystals. *Thin Solid Films* **1993**, *223*, 140–142.